Hybrid Three-Phase/Single-Phase Microgrid Architecture With Power Management Capabilities

Qiuye Sun, *Member, IEEE*, Jianguo Zhou, Josep M. Guerrero, *Fellow, IEEE*, and Huaguang Zhang, *Fellow, IEEE*

***Abstract*—With the fast proliferation of single-phase distributed generation (DG) units and loads integrated into residential microgrids, independent power sharing per phase and full use of the energy generated by DGs have become crucial. To address these issues, this paper proposes a hybrid microgrid architecture and its power management strategy. In this microgrid structure, a power sharing unit (PSU), composed of three single-phase back-to-back (SPBTB) converters, is proposed to be installed at the point of common coupling. The aim of the PSU is mainly to realize the power exchange and coordinated control of load power sharing among phases, as well as to allow full utilization of the energy generated by DGs. Meanwhile, the method combining the modified adaptive backstepping-sliding mode control approach and droop control is also proposed to design the SPBTB system controllers. With the application of the proposed PSU and its power management strategy, the loads among different phases can be properly supplied and the energy can be fully utilized, as well as obtaining better load sharing. Simulation and experimental results are provided to demonstrate the validity of the proposed hybrid microgrid structure and control.**

***Index Terms*—Adaptive backstepping-sliding-mode control, droop control, energy utilization, microgrid, power sharing.**

I. Introduction

With this high penetration of distributed generations (DGs), the concept of microgrids that can operate in either grid-connected or islanded modes is becoming more attractive [1]–[5]. A microgrid is a local controllable low-voltage distribution network consisting of a number of DGs, energy storage systems, and dispersed loads. DGs are often connected to the microgrid through power electronic interface converters, which are aimed at controlling the power injection while improving the power quality at the same time. Both the customers and power utilities can benefit from the microgrid concept, which can offer diversified energy options and high power quality and reliability [6]–[10]. Additionally, the use of low or zero emission generators in microgrids can increase the overall efficiency of energy utilization, dealing with environmental concerns, such as CO_2 emissions and reduction of dependence on conventional power generation [11], [12].

Accurate power management control among DGs is an important issue for the autonomous operation of microgrids. Typically, frequency and voltage droop control schemes are adopted to achieve power sharing among DGs without relying on communication [9], [10], [13]. Nevertheless, droop-controlled microgrids are prone to have some stability and power sharing accuracy problems due to complex feeder impedances and high control gains [14]–[16]. To address these problems, stability-constrained and adaptive decentralized droop controllers have been proposed in [17]–[19]. In [20], the reactive power sharing accuracy was improved with the consideration of impedance voltage drop, the DG local load effects, and the use of a virtual inductor loop. Methods based on virtual complex impedance loop and reactive power control error estimation were also proposed in [21] and [22], respectively. In order to mitigate the voltage and frequency deviations [23] produced by the conventional droop controllers, secondary control loops by using central PI compensators and decentralized networked control systems have been proposed [24]–[26]. The research works mentioned above, however, are mainly concentrated on DG control within a microgrid. Although much rarely seen, droop control applied to interlinked microgrids using back-to-back (BTB) converters can be found in [27]–[29], where, with the bidirectional control of the power flow, the specific amount of active and reactive power between utility and microgrid can be facilitated.

It is worth noting that the aforementioned research works were mostly confined to three-phase microgrid system and little work has been done and reported in the area of load power sharing and power flow control in single-phase microgrids, especially interlinked single-phase microgrids. Commonly, in a real microgrid, single-phase DG units are very common, and a growing number of single-phase DGs are being installed in microgrids [30]–[35]. Nevertheless, methods applied in three-phase systems cannot be directly applied in single-phase ones.

The operation and reactive power compensation of the single-phase microsources by using STATCOM were proposed and discussed in [30] and [31], respectively. In traction power system, single-phase BTB converters were utilized to achieve active power balancing, reactive power compensation, and harmonic mitigation [32]. Additionally, the active filtering strategy was also researched for the single-phase high-frequency ac microgrid in [33]. Further, a power sharing approach for islanding single-phase microgrid was proposed by using virtual impedance at fundamental and selective harmonic frequencies, trading-off DG terminal voltage THD and harmonic current

Manuscript received July 31, 2014; revised October 11, 2014; accepted November 28, 2014. Date of publication December 12, 2014; date of current version May 22, 2015. This work was supported by the National Natural Science Foundation of China under Grants 61433004 and 61034005, the National High Technology Research and Development Program of China (2012AA040104), the Fundamental Research Funds for the Central Universities (N130104001), and IAPI Fundamental Research Funds (2013ZCX14). Recommended for publication by Associate Editor B. Semail.

Q. Sun and J. Zhou are with the School of Information Science and Engineering, Northeastern University, Shenyang 110819, China (e-mail: sunqiuye@mail.neu.edu.cn; JianguoZhou.NEU@gmail.com).

J. M. Guerrero is with the Department of Energy Technology, Aalborg University, 9220 Aalborg East, Denmark (e-mail: joz@et.aau.dk).

H. Zhang is with the School of Information Science and Engineering, Northeastern University, Shenyang 110819, China and also with the Key Laboratory of Integrated Automation of Process Industry, Northeastern University, National Education Ministry, Shenyang 110819, China (e-mail: hgzhang@ieee.org).

Color versions of one or more of the figures in this paper are available online at http://ieeexplore.ieee.org.

Digital Object Identifier 10.1109/TPEL.2014.2379925

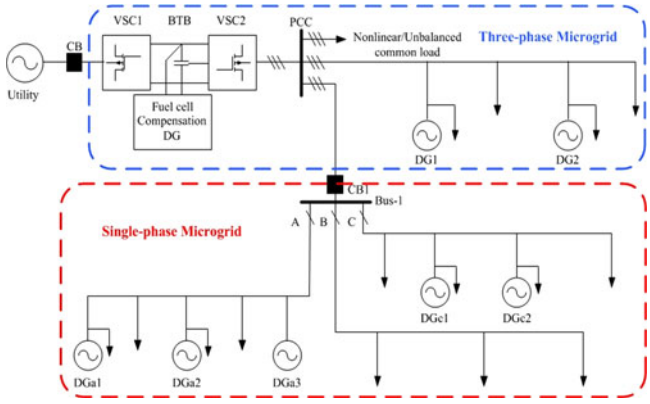

Fig. 1. Structure of the microgrid system under consideration.

sharing [34]. However, all these works were mainly focused on power quality issues.

Regarding bidirectionality in terms of power flow, a modular multilevel cascade BTB system with particular focus on control, design and performances has been discussed by Akagi in [28]. This BTB system characterized by the use of multiple bidirectional isolated dc/dc converters was connected between two 6.6 kV feeders, which can realize directional power flow control between feeders. Other applications of rural microgrids connected to the grid by means of a BTB converter can be found in [27] and [39]. However, only three-phase centralized system was discussed in this BTB application.

For the best knowledge of the authors, no research works have been reported about the power sharing and power flow control among individual phases of three-phase microgrids. In order to achieve it, a power sharing unit (PSU) and its operation and power management strategy are proposed in this paper. At first, the structure and operation principle of the proposed PSU is presented in detail in Section II. Section III presents the design of the internal and external control loops of the PSU. Section IV provides simulation and experimental results to demonstrate the effectiveness of the proposed PSU and power management. Finally, Section V gives the conclusion.

II. Structure and Operation Principles of the Proposed PSU

Fig. 1 shows the microgrid system under consideration, in which both three-phase and single-phase microgrids areas are connected to the utility grid through a three-phase BTB converter. Note that phase-A and phase-C contain DG units and some local loads, while phase-B has no DGs but loads. In such a configuration, even if the power generated by these DGs is larger than the load power demand in the two phases, the loads in the other phase (phase-B) will not be supplied when the single-phase microgrid is disconnected from the utility grid (CB0 open).

In the microgrid system, two operation modes, grid-connected and islanded modes are considered. Particularly, it should be noted that the operation mode and the control of the single-phase and three-phase microgrid areas are independent in islanded mode, when CB0 is open, as shown in Fig. 2.

In grid-connected mode, the single-phase microgrid, although there is no DG installed in phase-B, the load power demand in

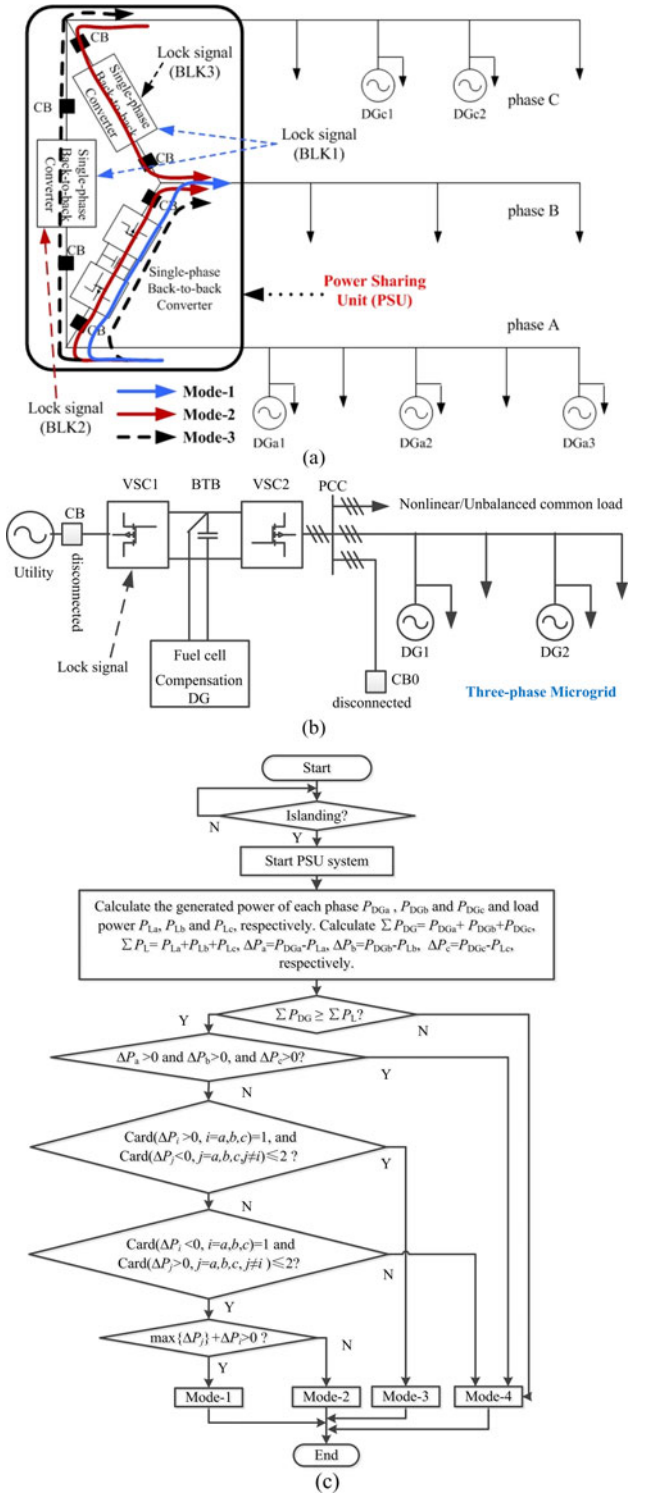

Fig. 2. Detailed schematic diagram of the microgrid: (a) single-phase and (b) three-phase parts; (c) flow-chart for different operating modes.

phase-B can be supplied by the utility grid. Nevertheless, when the microgrid is disconnected from the utility grid (CB open), the three-phase and single-phase microgrid areas will operate in islanded mode. Considering that the point of common coupling (PCC) voltage can be unbalanced and distorted seriously at the same time, independent operation of the three-phase and

single-phase microgrids is preferred (CB0 open). In this case, the loads in phase-B will lose the power supply and may not operate normally unless they can be supplied by some other power source. On the other hand, the power generated by DGs in phase-A and phase-C can be adequate, but will be restricted by the load power demand. So that the renewable energy such as wind or solar will be wasted. Additionally, it should be noted that the installation of DG such as rooftop PV system is determined by customers, including the unbalance situation in which few DGs are interfaced to one phase while other phases may be connected to a number of DGs. It should be emphasized that such microgrids widely exist in practice, such as residential customers in remote rural areas, multiple neighboring communities, and business districts. By taking residential customers in remote rural areas as an example, they usually suffer from low power quality and low reliability of power supply, due to the long distances from main power stations, large grid impedances, and weak grid voltage. However, renewable energy resources such as wind energy and solar energy in these areas are often adequate, thus small DGs can be installed near to the point of consumption. However, DGs cannot always be installed in some areas due to geographical factors. Consequently, sometimes it is necessary to develop an appropriate strategy to guarantee the power supply quality and availability of these areas where DGs are not installed or the capacity of DGs is small [27], [41].

Therefore, a PSU, as shown in Fig. 2(a), installed at Bus-1 (see Fig. 1) is proposed to overcome this problem. The structure and the principle of operation modes are presented in Fig. 2(a), where the PSU, which is composed of three voltage-source-based single-phase BTB converters which are delta connected, enables the power generated by DGs to be transmitted from one phase to another, ensuring the loads supplied uninterruptedly. Although a star structure would save three converters, the reason why a delta-connected structure rather than the star structure is considered in this paper mainly could be summarized as follows. *1) Higher reliability*: the fault tolerance is higher since in case of star connection, the power exchange between two phases would not be achieved when dc-link faults are happened. This scenario can be avoided by using the delta-connected structure even if the dc-link of one of the BTB converters fails. Power exchange between two phases may be realized through the other two BTB converters. *2) Smaller dc-link capacitance* is needed to achieve similar performances for the same amount of transferred power from one phase to the other two phases. *3) Hot-swap capability*: It is easier and more flexible to maintain the delta-connected PSU compared to the star-connected PSU. Within the delta-connected PSU, only one BTB converter should be stopped and maintained with proper control and protection strategy when faults happens to the dc-link or VSC, while the whole PSU equipment will be stopped for the star structure.

We assume that the capacity of DGs in phase-A is larger than that of phase-C, and that load of phase-C is larger than that of phase-A relatively. The PSU system depending on the power requirements in the microgrid can run in different modes: mode-1, load power demand in phase-B is supplied by DGs in phase-A; mode-2, load power demand in phase-B is supplied and shared coordinately by DGs in phase-A and phase-C; mode-3, load power demand in phase-B and phase-C is supplied by DGs in phase-A; mode-4, the PSU will be out of operation or locked

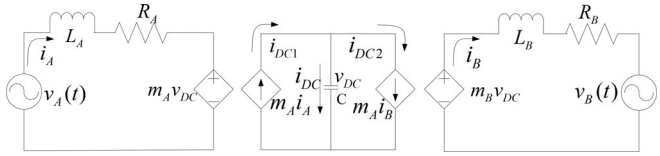

Fig. 3. Equivalent circuit of SPBTB.

and no power will be transferred. Specifically, in mode-1 shown in Fig. 2(a) with blue lines, loads in phase-B are shared only by DGs in phase-A through the SPBTB1 in the PSU since the power generated by DGs in phase-C can just meet load demand in its phase. In this case, SPBTB2 and SPBTB3 will be blocked with the corresponding signal BLK1 for the sake of safety and efficiency. When the power transmitted from phase-A cannot meet the power demand in phase-B and the power generated by DGs in phase-C is more than its phase load demand, the operation of the PSU will be changed from mode-1 to mode-2 shown in Fig. 2(a) with solid red lines. This mode can provide more reliable power supply and coordinated load power sharing realized by droop controllers for phase-B loads by DGs in phase-A and phase-C through SPBTB1 and SPBTB2 of the PSU. The SPBTB3 will be locked with the input signal BLK2. When power generated by DGs in phase-C is less than the power demand, the operation of the PSU will be changed to mode-3 shown in Fig. 2(a) with black-dashed lines. In this mode, DGs in phase-A will not only share the load power of phase-B, but also share the rest power requirement of phase-C. The SPBTB2 will be locked with the input signal BLK3 in this mode. When power generated by DGs in phase-A and phase-C just can meet the load demands of phase-A and phase-C, respectively, the operation of the PSU will be changed to mode-4. In this mode, the PSU will not transmit any power and will be stopped or locked. The situation is similar to that of phase-B if there is no DG installed in phase-A or phase-C. Fig. 2(c) shows the flowchart indicating the choices for showing the different operating modes.

Coordinated load power sharing control and power flow exchange among phases can be realized with the application of the proposed PSU in the microgrid, ensuring the loads supplied reliably, flexibly, and uninterruptedly and achieving higher efficiency of energy utilization in islanded mode under the condition that the whole generated power of three phases can meet the whole load demand. Application of the PSU in such microgrids is helpful to enhance power supply reliability, flexibility for residential customers in remote rural areas, multiple neighboring communities, and business districts in practice. Additionally, it also allows improving efficiency of energy utilization and save investments of transmission and distribution. In the following, we mainly focus on modeling and nonlinear controller design of SPBTB of PSU for the power sharing.

III. Modeling and Control Design of SPBTB of PSU

A. Modeling of SPBTB

The modeling of SPBTB system is based on the principal circuit analysis and voltage and current equations for storage elements known as state equation. The equivalent circuit of SPBTB is shown in Fig. 3.

Although *d-q* transformation and controller design in rotating coordinates are simple and powerful with respect to improving performance at the fundamental frequency, it is not directly applicable to single-phase power converters. Single-phase *d-q* transformation method [36] is adopted in this paper, and then the model of the SPBTB converter in the synchronous *d-q* reference frame is given as

$$\begin{cases} \dfrac{di_{Ad}}{dt} = -\dfrac{R_A}{L_A} i_{Ad} + \omega_A i_{Aq} + \dfrac{1}{L_A}\left(v_{Ad} - v_{\mathrm{DC}} m_{Ad}\right) \\ \dfrac{di_{Aq}}{dt} = -\dfrac{R_A}{L_A} i_{Aq} - \omega_A i_{Ad} + \dfrac{1}{L_A}\left(v_{Aq} - v_{\mathrm{DC}} m_{Aq}\right) \\ \dfrac{dv_{\mathrm{DC}}^2}{dt} = \dfrac{3}{C}\left(v_{Ad} i_{Ad} + v_{Aq} i_{Aq}\right) - \dfrac{2v_{\mathrm{DC}}^2}{R_p C} - \dfrac{2P_{\mathrm{load}}}{C} \end{cases} \tag{1}$$

$$\begin{cases} \dfrac{di_{Bd}}{dt} = -\dfrac{R_B}{L_B} i_{Bd} + \omega_B i_{Bq} + \dfrac{1}{L_B}\left(v_{\mathrm{DC}} m_{Bd} - v_{Bd}\right) \\ \dfrac{di_{Bq}}{dt} = -\dfrac{R_B}{L_B} i_{Bq} - \omega_B i_{Bd} + \dfrac{1}{L_B}\left(v_{\mathrm{DC}} m_{Bq} - v_{Bq}\right) \end{cases} \tag{2}$$

where m_{Ad}, m_{Aq}, m_{Bd}, and m_{Bq} are the modulation index, R_p is converter loss resistor, ω_A and ω_B are angular frequencies of two microgrids, respectively. Obviously, the above mathematical model of SPBTB is nonlinear.

Taking uncertainties into account, we can write the system (1) as follows:

$$\dot{x} = \bar{f}(x) + \Delta f(x) + \sum_{i=1}^{m} g_i(x) u_i \tag{3}$$

where the calculation methods of $\bar{f}(x)$, $\Delta f(x)$, $g_i(x)$, and u_i are given in Appendix A. we choose the output variables as

$$y = h(x) = \begin{bmatrix} v_{\mathrm{DC}}^2 \\ L_f h_1(x) \\ i_{Ad} \end{bmatrix}. \tag{4}$$

According to the derivation rule of Lee derivative [37] and the constructed new control inputs

$$\begin{bmatrix} \bar{u}_d \\ \bar{u}_q \end{bmatrix} = \begin{bmatrix} L_{g_1} L_{\bar{f}} h_1(x) u_d + L_{g_2} L_{\bar{f}} h_1(x) u_q \\ L_{g_1} h_2(x) u_d + L_{g_2} h_2(x) u_q \end{bmatrix}. \tag{5}$$

The dynamic model of the system (1) in the new coordinate can be written as follows:

$$\begin{cases} \dot{y}_1 = f_1(y_1) + G_1 y_2 + \phi_1^T(y_1)\theta \\ \dot{y}_1 = f_2(y_1, y_2) + G_2 u_d + \phi_2^T(y_1, y_2)\theta \end{cases} \tag{6}$$

$$\dot{y}_3 = f_3(y_3) + G_3 \bar{u}_q + \phi_3^T(y_3)\theta \tag{7}$$

where the new system (6) and (7) are the decoupled subsystems which are strict feedback form, respectively.

Using the similar approach, the dynamic model of system (2) in the new coordinate can also be obtained

$$\begin{cases} \dot{y}_4 = L_f h_4(x) + L_{g4} h_4(x) u_{d1} \\ \dot{y}_5 = L_f h_5(x) + L_{g5} h_5(x) u_{q1}. \end{cases} \tag{8}$$

The calculation methods of all terms in (4) to (8) are given in Appendix B.

B. Design of Nonlinear Controller of SPBTB

The control of the VSC-based SPBTB in the PSU is the key problem. Currently, the PI controllers and proportional multiresonant controllers are usually applied to the inverter-based microgrid, as well as droop control method. But recently, adaptive backstepping method is applied to the power electronic system [38], [39], which allows the designer to incorporate most system nonlinearities and uncertainties in the design of the controller [40]. The modified backstepping control method has been utilized to design the controller of BTB VSC system which is applied in HVDC, wind generation system, and hybrid power system such as transmission transformer (partial) bypass. On the other hand, sliding mode control is an effective robust control method due to the invariance for the disturbance and uncertain parameters [42]. A novel modified adaptive backstepping-sliding mode control approach is therefore applied to design the nonlinear controller of PSU. This approach not only can overcome the system nonlinearities and uncertainties, but also improve the performance of robustness.

In the SPBTB of the PSU system, one converter controls the dc-link voltage and supports its reactive power and the other one controls the active and reactive powers. The overall structure of the control system of the SPBTB in the PSU system is shown in Fig. 4 where the control system mainly includes dc-link voltage controller, modified adaptive backstepping controller and droop controller, which are described in detail in the following.

The controller design steps are given in the following. First, the controller design of VSC1 is conducted.

Step 1) For the subsystem (6), the tracking error is defined by

$$z_1 = y_1 - y_{1\mathrm{ref}}. \tag{9}$$

Then, the dynamics is given by

$$\dot{z}_1 = \dot{y}_1 - \dot{y}_{1\mathrm{ref}} = f_1(y_1) + G_1 y_2 + \phi_1^T(y_1)\theta - \dot{y}_{1\mathrm{ref}}. \tag{10}$$

To start backstepping, y_2 is chosen as the virtual control input variable, and we define another tracking error $z_2 = y_2 - \alpha_2$.

The virtual stabilizing function is chosen as

$$\alpha_2 = \frac{1}{G_1}\left[-f_1(y_1) - \phi_1^T(y_1)\hat{\theta} - c_1 z_1 + \dot{y}_{1\mathrm{ref}}\right]. \tag{11}$$

The parameter estimation error is defined as $\tilde{\theta} = \theta - \hat{\theta}$. Combining the definition of z_2, (10) can be written as

$$\dot{z}_1 = -c_1 z_1 + G_1 z_2 + \phi_1^T(y_1)\tilde{\theta}. \tag{12}$$

Step 2) The sliding surface is defined as $s = d_1 z_1 + z_2$, and the Lyapunov function is selected as

$$V_1 = \frac{1}{2} z_1^2 + \frac{1}{2} s_1^2 + \frac{1}{2}\tilde{\theta}^T \Gamma^{-1} \tilde{\theta}. \tag{13}$$

Then, the derivative of z_2 and the selected Lyapunov function is obtained as follows:

$$\begin{aligned} \dot{z}_2 = {} & f_2(y_1, y_2) + G_2 \bar{u}_d + \phi_2^T(y_1, y_2)\theta \\ & - \frac{d\alpha_2}{dy_1}(f_1(y_1) + G_1 y_2 + \phi_1^T(y_1)\theta) - \frac{d\alpha_2}{d\hat{\theta}}\dot{\hat{\theta}} \end{aligned} \tag{14}$$

$$\begin{aligned} \dot{V}_1 = {} & z_1 \dot{z}_1 + s\dot{s} - \tilde{\theta}^T \Gamma^{-1} \dot{\hat{\theta}} \\ = {} & -c_1 z_1^2 + G_1 z_1 z_2 + z_1 \phi_1^T(y_1)\tilde{\theta} - \tilde{\theta}^T \Gamma^{-1} \dot{\hat{\theta}} \end{aligned}$$

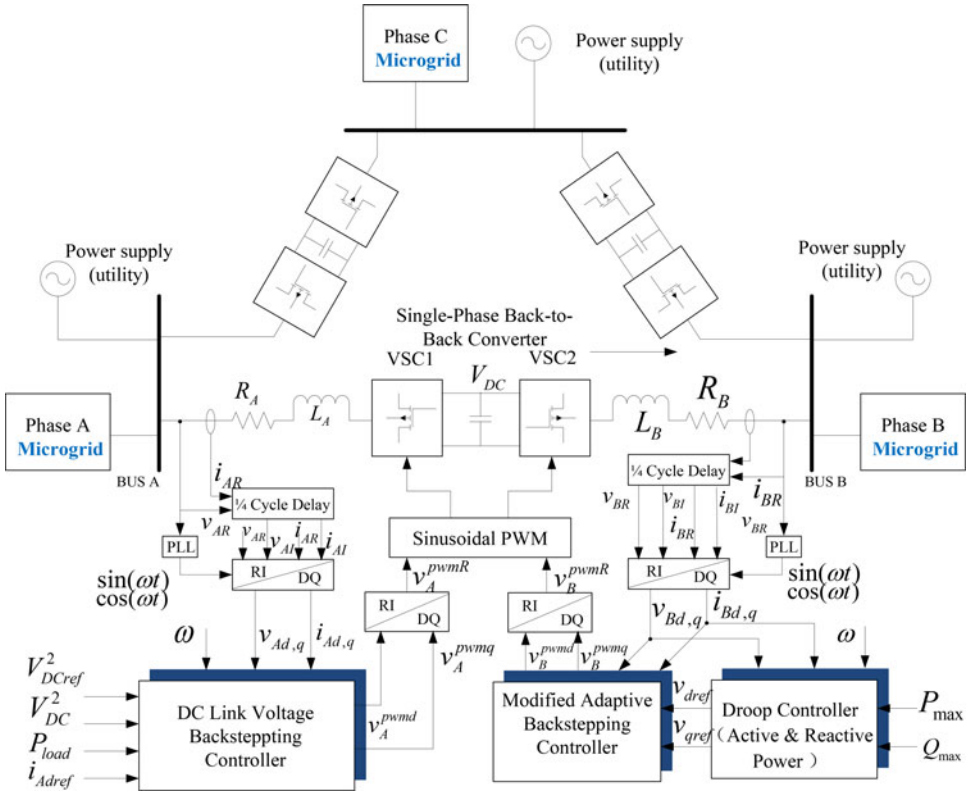

Fig. 4. Block diagram of the global control system.

$$+ s[-d_1 c_1 z_1 + d_1 G_1 z_2 + d_1 \phi_1^T(y_1)\tilde{\theta} + f_2(y_1, y_2) + G_2 \bar{u}_d + \phi_2^T(y_1, y_2)\theta - \frac{d\alpha_2}{dy_1}\begin{pmatrix} f_1(y_1) + G_1 y_2 \\ +\phi_1^T(y_1)\theta \end{pmatrix} - \frac{d\alpha_2}{d\hat{\theta}}\dot{\hat{\theta}}]. \quad (15)$$

The feedback control law and the parameter adaptation law can be designed as follows:

$$\bar{u}_d = \frac{1}{G_2}\begin{bmatrix} d_1 c_1 z_1 - d_1 G_1 z_2 - f_2(y_1, y_2) \\ -\phi_2^T(y_1, y_2)\hat{\theta} + \frac{d\alpha_2}{dy_1} \\ \left(f_1(y_1) + G_1 y_2 + \phi_1^T(y_1)\hat{\theta}\right) \\ +\frac{d\alpha_2}{d\hat{\theta}}\dot{\hat{\theta}} - \gamma s - G_1 z_1 z_2 / s \end{bmatrix} \quad (16)$$

$$\dot{\hat{\theta}}^T = \left[z_1 \phi_1^T(y_1) + s\left(d_1 \phi_1^T(y_1) + \phi_2^T(y_1, y_2) - \frac{d\alpha_2}{dy_1}\phi_1^T(y_1)\right)\right]\Gamma. \quad (17)$$

Combing (15)–(17), the derivative of Lyapunov function becomes

$$\dot{V}_1 = -c_1 z_1^2 - \gamma s^2. \quad (18)$$

With the suitable choices of $c_1 > 0$ and $\gamma > 0$, the requirement of $\dot{V}_1 \leq 0$ can be met.

For the subsystem (7), the tracking error is defined as

$$z_3 = y_3 - y_{3\mathrm{ref}} \quad (19)$$

then, the dynamics can be obtained

$$\dot{z}_3 = \dot{y}_3 - \dot{y}_{3\mathrm{ref}} = f_3(y_3) + G_3 \bar{u}_q + \phi_3^T(y_3)\theta - \dot{y}_{3\mathrm{ref}}. \quad (20)$$

We consider a new Lyapunov function as

$$V_2 = \frac{1}{2} z_3^2 \quad (21)$$

then the derivative of (21) is

$$\begin{aligned} \dot{V}_2 &= z_3 \dot{z}_3 \\ &= z_3\left(f_3(y_3) + G_3 \bar{u}_q + \phi_3^T(y_3)\theta - \dot{y}_{3\mathrm{ref}}\right) \\ &= z_3\left(f_3(y_3) + G_3 \bar{u}_q - \dot{y}_{3\mathrm{ref}}\right). \end{aligned} \quad (22)$$

The control law is therefore chosen as

$$\bar{u}_q = \frac{1}{G_3}\left[-f_3(y_3) + \dot{y}_{3\mathrm{ref}} - c_3 z_3\right]. \quad (23)$$

Substituting (23) into (22), the requirement $\dot{V}_2 = -c_3 z_3^2 \leq 0$ can be met with the suitable choice of $c_3 > 0$.

In the following, the design of the controller of VSC2 that controls the active and reactive power sharing between two ac systems will be discussed in detail. Specifically, the inner-loop controller will be designed with the aforementioned modified adaptive backstepping-sliding mode control method.

The controller design of subsystem (8) is as follows.

The tracking errors are defined by

$$\begin{cases} z_4 = y_4 - y_{4\mathrm{ref}} \\ z_5 = y_5 - y_{5\mathrm{ref}} \end{cases} \quad (24)$$

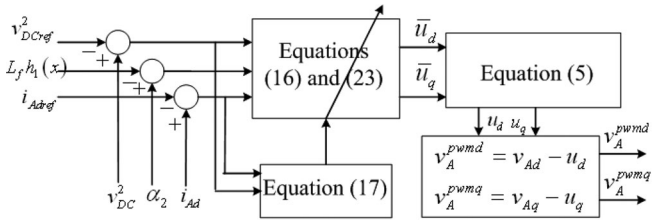

Fig. 5. Block diagram of the dc-link voltage control system of VSC1.

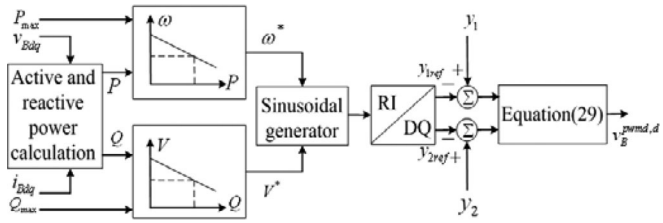

Fig. 6. Detailed block diagram of the active and reactive power control system of VSC2.

and taking the time derivative of (24) yields

$$\begin{cases} \dot{z}_4 = \dot{y}_4 - \dot{y}_{4\mathrm{ref}} = L_f h_4(x) + L_{g4} h_4(x) u_{d1} - \dot{y}_{4\mathrm{ref}} \\ \dot{z}_5 = \dot{y}_5 - \dot{y}_{5\mathrm{ref}} = L_f h_5(x) + L_{g5} h_5(x) u_{q1} - \dot{y}_{5\mathrm{ref}}. \end{cases} \tag{25}$$

The Lyapunov function is given by

$$V = \frac{1}{2} z_4^2 + \frac{1}{2} z_5^2 \tag{26}$$

the derivative of the Lyapunov function is

$$\begin{aligned} \dot{V} = & \; z_4 \dot{z}_4 + z_5 \dot{z}_5 \\ = & \; z_4 (L_f h_4(x) + L_{g4} h_4(x) u_{d1} - \dot{y}_{4\mathrm{ref}}) \\ & + z_5 (L_f h_5(x) + L_{g5} h_5(x) u_{q1} - \dot{y}_{5\mathrm{ref}}). \end{aligned} \tag{27}$$

If we choose the feedback control laws as

$$\begin{aligned} u_{d1} = & \; \frac{1}{L_{g4} h_4(x)} [-L_f h_4(x) + \dot{y}_{4\mathrm{ref}} - c_4 z_4] \\ u_{q1} = & \; \frac{1}{L_{g5} h_5(x)} [-L_f h_5(x) + \dot{y}_{5\mathrm{ref}} - c_5 z_5] \end{aligned} \tag{28}$$

and with suitable choices of $c_4, c_5 > 0$, the derivative of the Lyapunov function can be given as

$$\dot{V} = -c_4 z_4^2 - c_5 z_5^2 \leq 0. \tag{29}$$

Since $\dot{V}$ is negative-definite, the states z_4 and z_5 can converge to zero, and the tracking requirements can be met.

C. Power Management Via Droop Control

To achieve coordinated load active and reactive power sharing among phases through the SPBTB-based PSU system, droop control method given in (30) is implemented to design the VSC outer-loop controller

$$\begin{aligned} \omega = & \; \omega_0 - m \cdot (P_0 - P) \\ E = & \; E_0 - n \cdot (Q_0 - Q) \end{aligned} \tag{30}$$

where m is the frequency droop coefficient, n is the voltage droop coefficient, ω_0 is the nominal frequency, E_0 is the rated phase voltage magnitude, P_0 and Q_0 are the active and reactive power rated capacity of the SPBTB converter. The droop coefficients m and n are taken proportional to rated power of SPBTBs for power sharing among them.

The block diagrams of the control system of the SPBTB converter are shown in Fig. 4. Specifically, the dc-link voltage controller of VSC1 is shown in Fig. 5. The controllers of VSC2 including droop controller are shown in Fig. 6. The controllers of VSC1 and VSC2 are mainly to maintain the dc-link voltage and to control the active and reactive power, respectively.

TABLE I
TEST SYSTEM AND CONTROLLER PARAMETERS

System Quantities	Values
Utility grid	
Frequency	50 Hz
Source voltage	380 V rms (L-L)
Feeder impedance	$R_S = 1\ \Omega, L_S = 0.5$ mH
DGs and SPBTB VSCs	
DC voltage	$V_{dc1} = V_{dc2} = V_{dc3} = 400$ V
Filter inductances	$L_{f1} = L_{f2} = L_{f3} = 1.35$ mH
and capacitances	$C_{f1} = C_{f2} = C_{f3} = 100\ \mu$F
Coupling impedance	$R_1 = R_2 = R_3 = 1\ \Omega, L_1 = L_2 = L_3 = 0.25$ mH
Rated capacity	$P_{RDGa1} = 14$ kW, $Q_{RDGa1} = 6$ kVar
	$P_{RDGa2} = 21$ kW, $Q_{RDGa2} = 9$ kVar
	$P_{\mathrm{RDGc1}} = 3$ kW, $Q_{\mathrm{RDGc1}} = 1.3$kVar
Overall efficiency the PSU	$84\% \sim 90\%$
Microgrid line impedance	$R_a = R_b = R_c = 0.5\Omega, L_a = L_b = L_c = 0.25$ mH
	$R_{a1} = R_{a2} = R_{b1} = R_{b2} = R_{c1} = R_{c2} = 0.5\ \Omega$
	$L_{a1} = L_{a2} = L_{b1} = L_{b2} = L_{c1} = L_{c2} = 0.25$ mH
Loads	$P_{L1} = 5$ kW, $Q_{L1} = 1$ kVar
	$P_{L2} = 2$ kW, $Q_{L2} = 1$ kVar
	$P_{L3} = 3$ kW, $Q_{L3} = 1$ kVar
	$P_{L4} = 9.5$ kW, $Q_{L4} = 3.12$ kVar
	$P_{L5} = 5$ kW, $Q_{L5} = 2$ kVar
	$P_{L6} = 4.5$ kW, $Q_{L6} = 1.12$ kVar
	$P_{L7} = 4$ kW, $Q_{L7} = 0.5$ kVar
Controllers of SPBTB VSCs	$m_1 = 6 \times 10^{-5}, n_1 = 1 \times 10^{-3}$
	$m_2 = 9 \times 10^{-5}, n_2 = 1.5 \times 10^{-3}$
	$m_3 = 6 \times 10^{-5}, n_3 = 1 \times 10^{-3}$
	$c_1 = 2, c_2 = 2, c_3 = 3, d_1 = 0.4, \Gamma = 0.5$

IV. SIMULATION RESULTS

To verify the effectiveness of the proposed strategies, simulation studies are carried out in MATLAB/SIMULINK (version 7.6). The single-phase microgrid test system with the proposed PSU is shown in Fig. 7, where two DGs are considered in phase-A of the microgrid, one DG in phase-C of the microgrid and no DGs in phase-B. Some key simulation parameters are listed in Table I. During the simulation, the microgrid is operating in the islanded mode, and various operating conditions with different load demands are considered.

The simulation considered in this paper includes five cases:

1) power flow from phase-A to phase-B;
2) power flow from phases A and C to phase-B;
3) power flow from phase-A to phase-C;

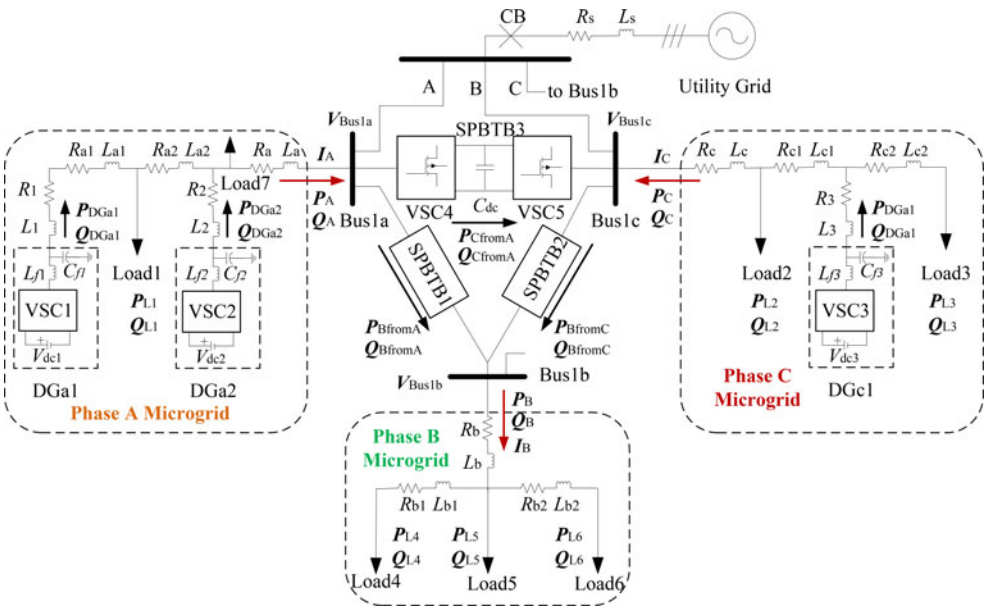

Fig. 7. Test single-phase microgrid with SPBTB.

4) voltage and frequency change in phase-A of the microgrid;
5) fault within one BTB converter.

Simulation studies are discussed for these five cases as follows.

A. Power Flow From Phase-A to Phase-B

In reality, one probable scenario would be that power generated by DGs in phase-C can only meet the power demand of its phase, while power generated by DGs in phase-A may be adequate enough to meet the load power demand of phase-B as well as that of phase-A. Under this circumstance, therefore, the load in phase-B can be supplied (or shared) by DGs in phase-A through the proposed PSU in islanded mode, resulting in reliable, uninterruptible power supply, and higher efficiency of renewable energy utilization. Due to the reasons mentioned above, power supply from phase-A to phase-B of the microgrid would be considered in this case.

Fig. 8 shows the active and reactive load power of both phase-A and phase-B shared by DGa1 and DGa2 and the power transmitted from phase-A to phase-B. Initially, the active and reactive load power demand of phase-B (P_B, Q_B) is 9.5 kw and 3.12 kvar, respectively, while that of phase-A (P_{L1}, Q_{L1}) is 5 kw and 1 kvar, respectively. As shown in Fig 8(a) and (b), a part of power generated by DGa1 and DGa2 has been transmitted from phase-A to phase-B, ensuring their normal operation in islanded mode. That is to say, DGa1 and DGa2 not only supply the power demand of phase-A but also supply the power demand of phase-B. At 0.6 s, the load power of phase-B is doubled, arriving at 19 kW and 6.24 kvar, and at 1.3 s, the load power of phase-A is changed to 9 kW and 1.5 kvar as shown in Fig. 8(a) and (b). It can be seen that the DGs can pick up the balance load demand and share it proportionally as desired through the PSU. It can also be seen that if the load power changed greatly, the slightly active power oscillation shown in Fig. 8(a) may occur, but it can be eliminated quickly after several cycles. On the other hand, the

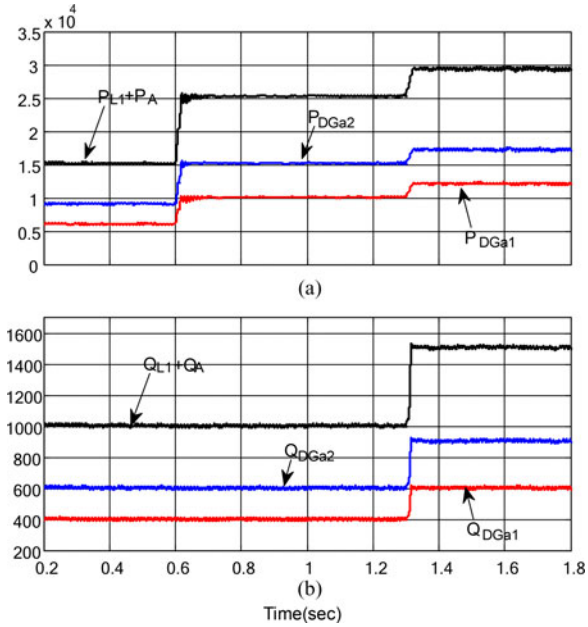

Fig. 8. Active and reactive power. (a) DG active power sharing (W). (b) DG reactive power sharing (var).

load active and reactive power of phase-B (P_B, Q_B) can remain almost constant while load power changed in phase-A. Fig. 9 shows the capacitor voltage of SPBTB1. The dc voltage reference is 400 V, and it can be seen that the voltage can keep at the reference value and that it has good robustness when the loads changed. With the application of PSU, the loads in phase-B can be supplied by DGs in other phases in the islanded mode.

B. Power Flow From Phase-A and Phase-C to Phase-B

In this case, the condition that the power demand of phase-B is supplied by DGs in both phase-A and phase-B of the microgrids

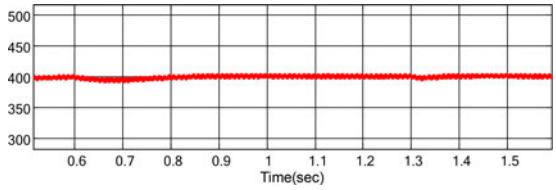

Fig. 9. Capacitor voltage of SPBTB1 (V).

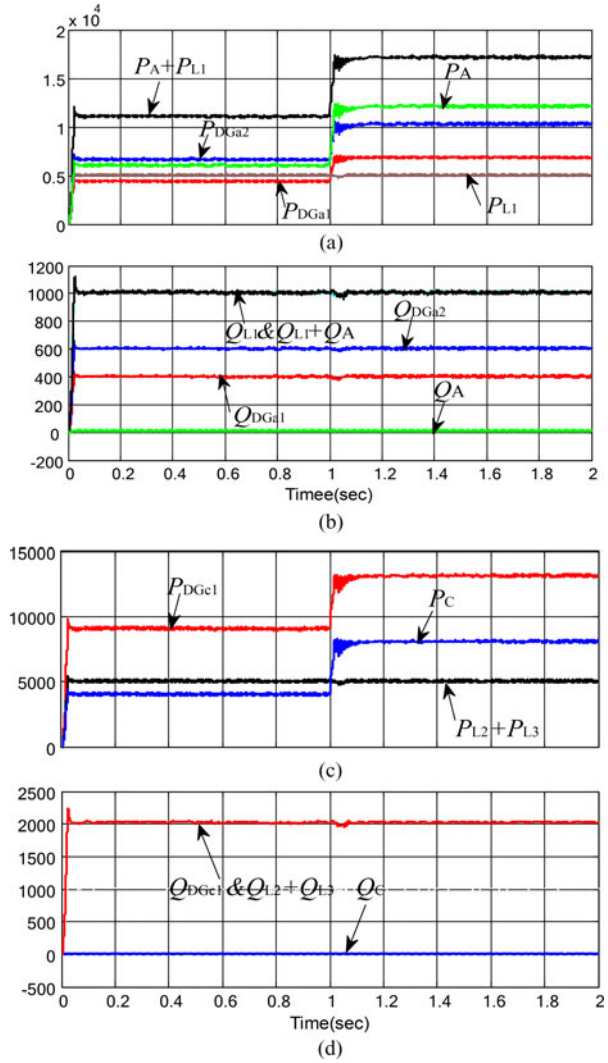

Fig. 10. Active and reactive power sharing among DGs. (a) and (c) active power sharing among DGa1, DGa2, and DGc1 (W). (b) and (d) reactive power sharing among DGa1, DGa2 and DGc1 (var).

through the PSU (SPBTB1 and SPBTB2) is considered, which means that in phase-A and phase-C, DGa1, DGa2, and DGc1 not only share the power demand of Load1, Load2, and Load3, but also share the load power of phase-B due to the adequate generation capacity of DGs. Under this consideration, the load power of phase-A (P_{L1}, Q_{L1}) and phase-C ($P_{L2}+P_{L3}, Q_{L2}+Q_{L3}$) are always remaining 5 kW, 1 kvar, and 5 kW, 2 kvar, respectively, while the load power of phase-B changes from 9.5 kW and 3.12 kvar to 19 kW and 6.24 kvar at 1 s. Figs. 10 and 11 show the active and reactive power sharing among DGs and power sharing between phase-A and phase-C of the

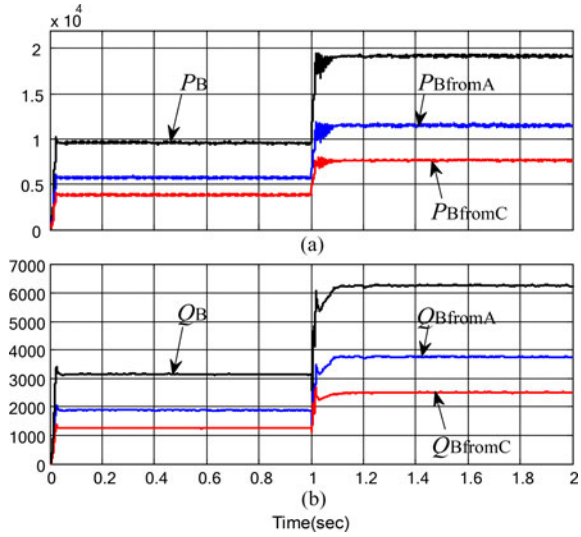

Fig. 11. Phase-B load power sharing between phase-A and phase-C of the microgrids. (a) Active power sharing (W). (b) Reactive power sharing (var).

microgrid, respectively. As shown in Fig. 11, at 1 s, the load power of phase-B (P_B, Q_B) is doubled, arriving at 19 kw and 6.24 kvar, and it can be seen that phase-A and phase-C of the single-phase microgrid can pick up the balance load demand quickly and share it proportionally as desired through SPBTB1 and SPBTB2 of the PSU system. The active and reactive power sharing (P_{BfromA}, P_{BfromC}, Q_{BfromA}, and Q_{BfromC}) is shown in Fig. 11(a) and (b), respectively. On the other hand, as shown in Fig. 10(a)–(d), it can be seen that regardless of the power changing of phase-B, the DGs (DGa1, DGa2, and DGc1) in phase-A and phase-C can track the power changing accurately and share it proportionally (P_{DGa1}, P_{DGa2}, P_{DGc1}, Q_{DGa1}, Q_{DGa2}, and Q_{DGc1}) and that the load power (P_{L1}, Q_{L1}, $P_{L2}+P_{L3}$, and $Q_{L2}+Q_{L3}$) of phase-A and phase-C remain almost undisturbed. We can see that using the PSU system, the loads in the phase where there is no DG installed can be shared by DGs in the other phases coordinately, resulting in normal operation of the load and enhanced reliability and flexibility of power supply in islanded mode. Additionally, higher efficiency of renewable energy utilization can be achieved with the application of the proposed PSU.

C. Power Flow From Phase-A to Phase-C

In this case, we assume that the power requirement of the load in phase-C is more than the power generated by the DGc1, while in phase-A, the power requirement is less than the power generated by DGa1 and DGa2, so the rest load power requirement in phase C microgrid can be supplied by phase-A of the microgrid through the PSU (SPBTB3). That is to say, the load power of phase-C is shared not only by DGc1 (phase-C) but also by DGa1and DGa2 (phase-A).

Figs. 12 and 13 show the active and reactive power among DGa1, DGa2, and DGc1. It can be seen that DGc1 can only generate the active and reactive power of 2 kw and 1 kvar, which is not adequate enough to balance the load demand, so the rest power demand of the load is supplied by phase-A through the SPBTB3 of the PSU (P_C, Q_C) (note that the power (P_C, Q_C)

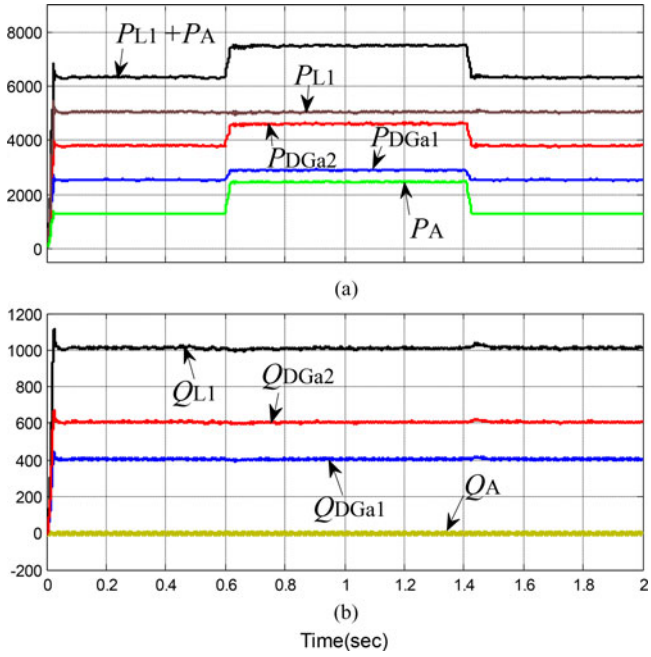

Fig. 12. Active and reactive power sharing between DGa1 and DGa2. (a) Active power sharing (W). (b) Reactive power sharing (var).

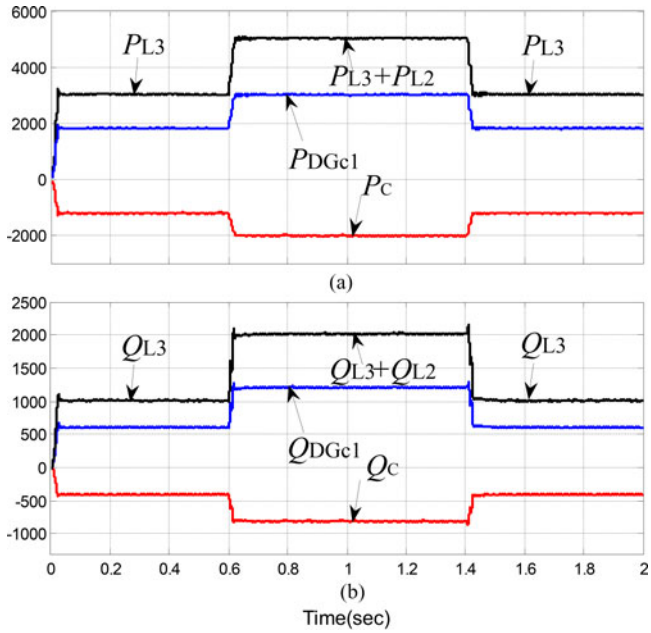

Fig. 13. Phase-C load power sharing between SPBTB3 and DGc1. (a) Active power sharing (W). (b) Reactive power sharing (var).

is less than zero indicates that the power energy is transmitted from phase-A to phase-C). At 0.6 s, the load of phase-C is doubled (Load2 is connected into the system) and at 1.4 s, it is changed back to the nominal value (Load2 is disconnected from the system). It can be seen that DGa1 and DGa2 (or SPBTB3) can pick up the balance load demand as desired (P_{DGa1}, P_{DGa2}, Q_{DGa1}, and Q_{DGa2}). It can also be seen that the active and reactive power (P_{L1}, Q_{L1}) of phase-A can remain almost constant regardless of the load power changing of phase-C.

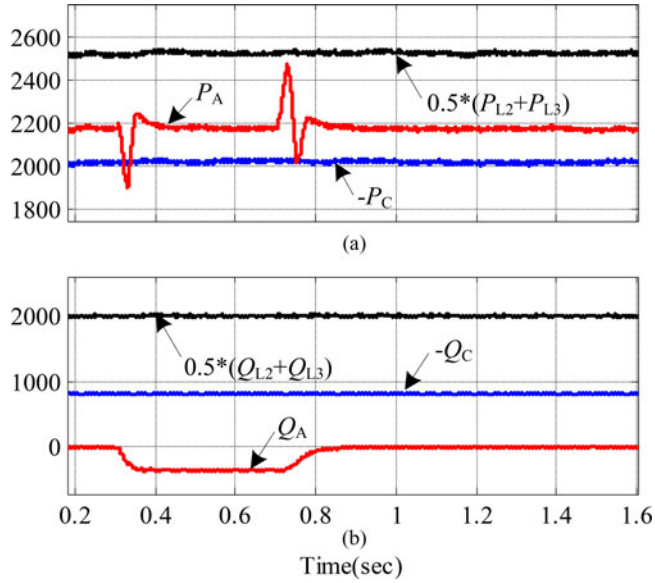

Fig. 14. Active and reactive power response during voltage fluctuation. (a) active power response (W) and (b) reactive power response (var).

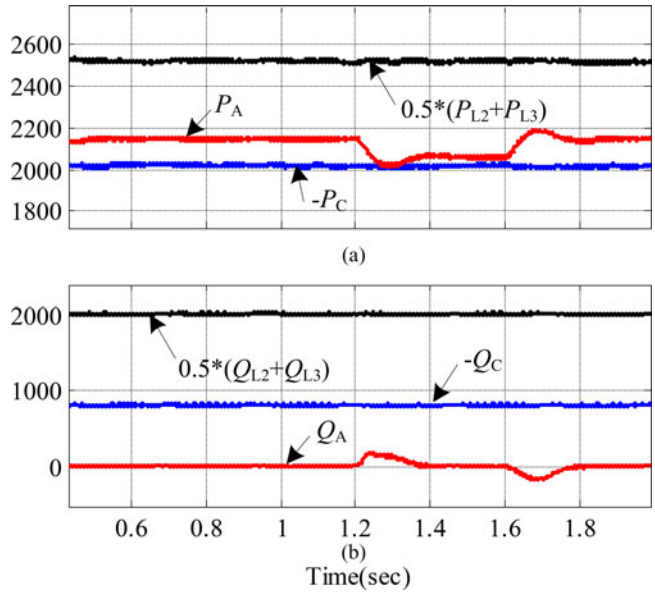

Fig. 15. Active and reactive power response during frequency fluctuation. (a) Active power response (W). (b) Reactive power response (var).

D. Voltage and Frequency Change in Phase-A of the Microgrid

It is known that one outstanding advantage is that due to the isolation provided by BTB converter connection, the voltage and frequency fluctuation in one phase will not impact on another one. Voltage and frequency fluctuations occurred in phase-A of the single-phase microgrid at different periods of time is therefore considered in this case. The system response for voltage and frequency fluctuations is shown in Figs. 14 and 15, respectively.

As shown in Fig. 14, a 50% voltage sag at V_{Bus1a} (shown in Fig. 7) in phase-A of the microgrid occurs at 0.3 s and is removed after 0.4 s. It can be seen that the load power ($P_{\mathrm{L2}}+P_{\mathrm{L3}}$,

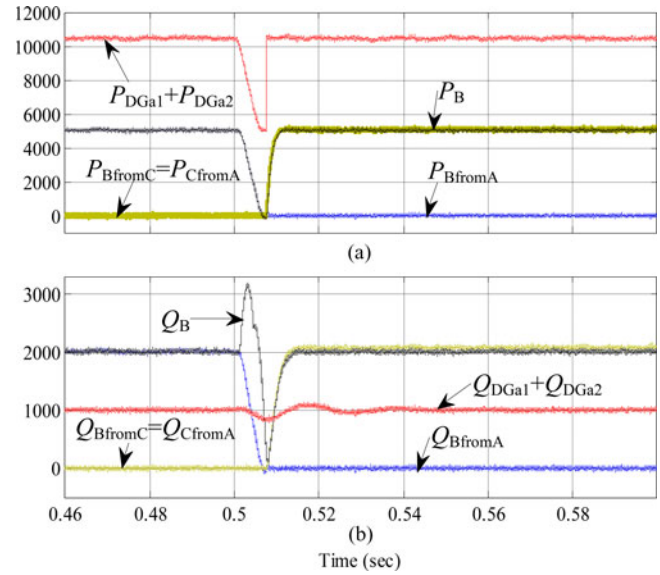

Fig. 16. Active and reactive power response when SPBTB1 fails. (a) Active power response (W) and (b) Reactive power response (var).

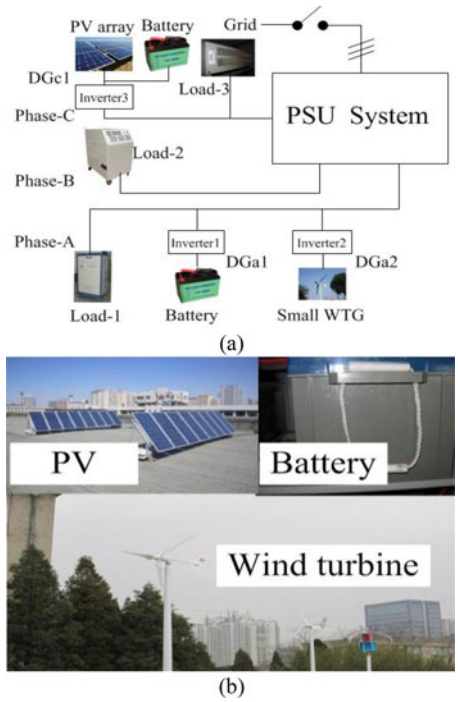

Fig. 17. Experimental verification. (a) Schematic diagram of hardware. (b) Laboratory setup.

$Q_{L2}+Q_{L3}$) of phase-C and the injected power (P_C, Q_C) to phase-C have not been impacted by the voltage sag occurred in phase-A, remaining almost undisturbed. As shown in Fig. 15, the frequency of phase-A dropped by 0.5% at 1.2 s, and at 1.6 s, it comes back to its normal value. It can be seen that while the injected power (P_A, Q_A) from phase-A to the PSU (SPBTB3) fluctuate, the load power ($P_{L2}+P_{L3}, Q_{L2}+Q_{L3}$) of phase-C and the injected power (P_C, Q_C) from SPBTB3 to phase-C remain almost undisturbed.

E. Fault Within One BTB Converter

In order to verify the reliability of the PSU system, the scenario of an internal fault within one BTB converter, which produced its automatic disconnection, has been simulated. In that case the load demand in phase-B is only supplied by the DGs connected in phase-A. Fig. 16 shows the system response when a fault occurs in SPBTB1. As shown in Fig. 16, the active and reactive power (P_{BfromA}, Q_{BfromA}) transferred through SPBTB1 drops quickly to zero due to this fault at 0.5 s. To maintain the power supplied to loads in phase-B, SPBTB2 and SPBTB2 are then transferring the demanded power ($P_{\mathrm{BfromC}} = P_{\mathrm{CfromA}}$, $Q_{\mathrm{BfromC}} = Q_{\mathrm{CfromA}}$) to phase-B at the same time. It can be seen that the loads in phase-B can be pretty well supplied by DGs in phase-A through the PSU system, in spite of the internal fault and subsequent disconnection of one of the BTB converters (in this case SPBTB1). Therefore, power supply with high availability and reliability can be guaranteed by using the proposed PSU system.

V. Experimental Results

To verify the effectiveness of the developed PSU-based microgrid and the proposed control strategy, experiments are also conducted on a scaled laboratory setup. The experimental test microgrid is composed of three identical single-phase H-bridge inverters, a PSU system composed of three single-phase BTB converters that are delta connected loads and the dc-link voltages of these inverters. The dc-link voltages are provided by PV array, battery bank, and small wind turbine generators (WTG) through dc–dc/ac–dc converters, respectively. The PV array is located on the top of the building, the WTG are installed in the vicinity of the building and the batteries are installed in the lab. Two of these inverters to interface battery bank and small WTG are installed in phase-A, the other one to interface PV array is installed in phase-C and there is no inverter installed in phase-B of the microgrid. Adjustable loads are connected

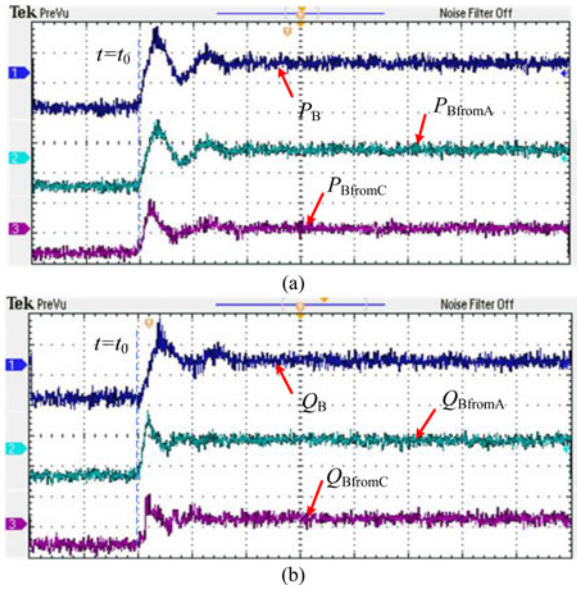

Fig. 18. Transient response of SPBTB1 and SPBTB2 with a step change of 5 kW and 2 kvar of load-3 in phase-B: (a) active power (W) and (b) reactive power (var).

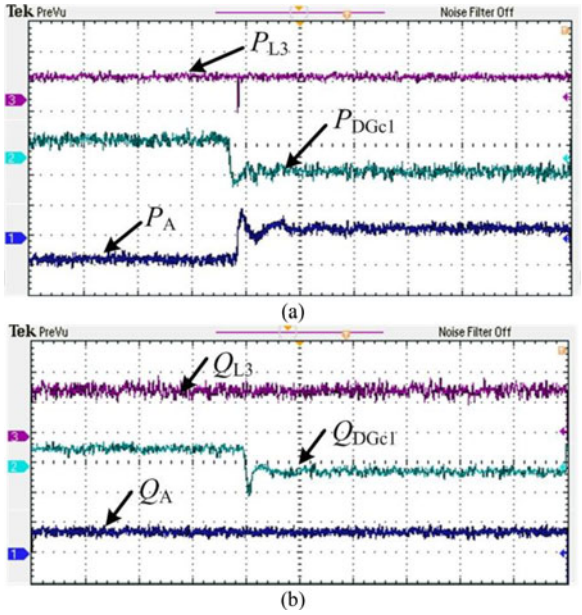

Fig. 19. Transient response of DGs and load-3: (a) active power (W) and reactive power (var).

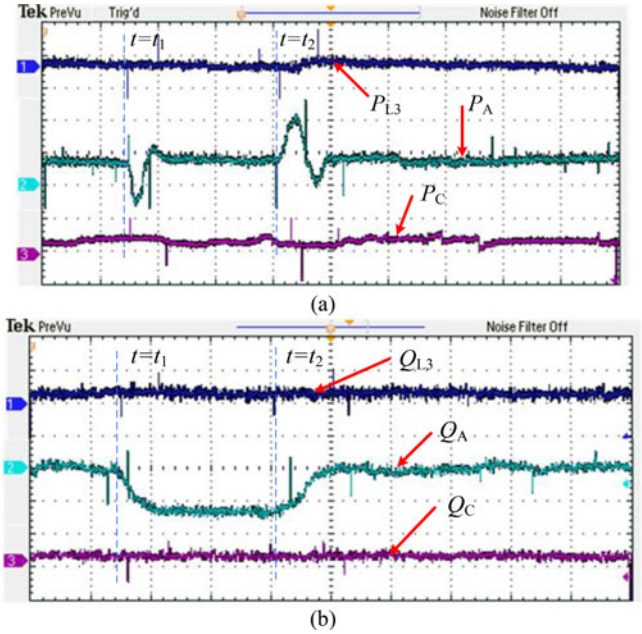

Fig. 20. Transient response during a voltage sag: (a) active power (W) and (b) reactive power (var).

to each phase. The laboratory setup implemented is shown in Fig. 17, and the experimental system parameters are given in Appendix C (TABLE II).

In this Section, two experiments with different operating conditions are conducted.

First, the load power demand of phase-B is shared by DGs in both phase-A and phase-C through SPBTB1 and SPBTB2 of the PSU system, proportionally. The ratio of the droop gains of SPBTB1 and SPBTB2 is 2:3.

Fig. 18 shows the fundamental output active and reactive power (P_{BfromA}, P_{BfromC}, Q_{BfromA}, and Q_{BfromC}) response of SPBTB1 and SPBTB2, respectively, as well as the load power in

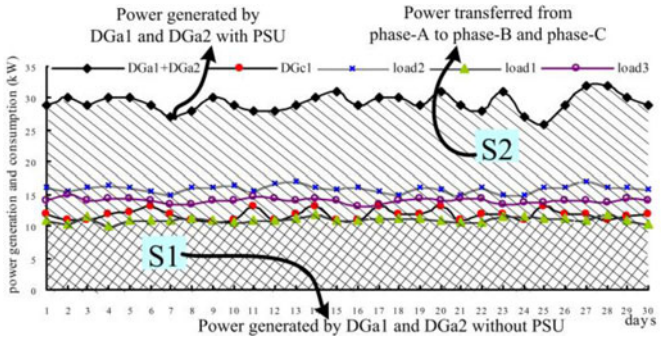

Fig. 21. Power generation and consumption.

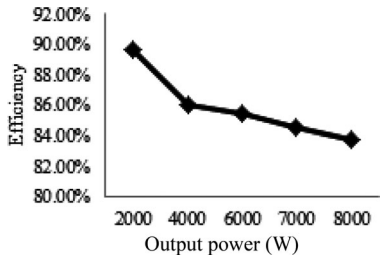

Fig. 22. Efficiency of the PSU prototype.

phase-B of the microgrid. At $t = t_0$ s, a step change of 2.5 kW active power and 1 kVar reactive power of load-2 in phase-B was excited (initially 2.5 kW and 1 kVar). From the experimental results presented in Fig. 18, it can be seen that the load in phase-B can be supplied by DGs in phase-A and phase-C of the microgrids through BTB converters of the PSU system, proportionally. That is to say, in the islanded mode, if the power generated by DGs is less than the power demand in this phase while the power generated by DGs is more than the load power demand in other phases, the rest power demand can be supplied by DGs in other phases through the PSU system. By doing so, the loads in phase-B microgrid can be supplied uninterruptedly and flexibly when the microgrid runs in islanded mode. With the application of the PSU, the coordinated load active and reactive power sharing can be realized among phases, and the energy generated by DGs also can be fully utilized.

In the following, the power supply from phase-A to phase-C through the PSU system is conducted with the consideration of one probable scenario that DGc1 cannot supply load-3 in phase-C normally due to the weather conditions in islanded mode while DGa1 and DGa2 may have enough power to supply load-3 in phase-C as well as load-1 in phase-A. Because that unlike small WTG, PV-based DG cannot generate power at night. The active and reactive power response of DGc1 is shown in Fig. 19, where the power flown from phase-A to phase-C is also presented. As shown in Fig. 19, in order to maintain the normal operation of load-3, DGa1 and DGa2 will share the rest power demand of load-3 through the PSU system quickly when DGc1 cannot meet the power demand of load-3. Although the active and reactive power generated by DGc1 has reduced, the operation of load-3 remains undisturbed due to the application of the PSU.

To investigate the power response during the voltage sag, the experiment is also conducted. In this test, a part of load power demand of phase-C is shared by DGs in phase-A through the PSU system. During the test, at $t = t_1$ s, a 20% voltage sag at

the input terminal of the PSU in phase-A occurred and at $t = t_2$ s, the voltage sag is removed. The active and reactive load power (P_{L3}, Q_{L3}) of phase-C, the input power (P_A, Q_A) of the PSU and the injected power (P_C, Q_C) to phase-C during this voltage sag are presented in Fig. 20. As it can be seen, the load power of phase-C and the injected power to phase-C remain almost undisturbed during the voltage sag. This is the advantage of the application of BTB converters which provide the isolation between phases thereby ensuring the normal operation of the system.

In order to observe the efficiency of the application of PSU system, daily power generation of DGs and power consumption of loads have been obtained for 30 days continuously, which is shown in Fig. 21. From the results, it can be seen that if there is no PSU implemented in the microgrid, DGa1 and DGa2 can only supply the load in phase-A and the power generation (S1 shown in Fig. 21) is constrained by load-1 even the weather condition is good enough to supply the load in phase-B and phase-C. So in this condition, without power supply, load-2 in phase-B cannot operate normally in islanded mode. The abundant primary energy will be wasted. However, with the application of the proposed PSU, the abundant primary energy will be conductive to generate more electricity by DGa1 and DGa2 to supply load-2 in phase-B as well as part power of load-1 in phase-C through PSU in the islanded mode, achieving higher efficiency of the renewable energy utilization. The efficiency of the proposed PSU prototype is also measured experimentally. The measured efficiency curve is shown in Fig. 22, which shows that the overall efficiency of the system ranges from 83.5% to 89.6%. The efficiency improvement of the system could be studied in the future by choosing global optimized switching frequency, etc.

VI. Conclusion

In this paper, the operation and energy management control strategy is proposed for the PSU-based hybrid microgrid in the islanded mode. The PSU composed of three SPBTB converters that are delta connected is installed at the PCC bus. The aim of the PSU is mainly to realize the coordinated control of load power sharing among different phases. The structure, principle, and operation of the proposed PSU installed in the hybrid microgrid are discussed in detail first. Then, the design of the PSU nonlinear controllers is also presented by using the droop control method and the modified adaptive backstepping-sliding mode control approach, which can achieve the coordinated power sharing and enhance robustness. With the application of the proposed PSU, it is not only the coordinated load power sharing and power flow control among phases that can be realized, but also the load that can be supplied uninterruptedly. Besides, the efficiency of energy utilization can be greatly increased and the voltage and frequency isolation can be provided by the PSU. Finally, the simulation and experimental results demonstrate the validity of the proposed application of PSU in the hybrid microgrid and its energy management control scheme. The proposed delta-connected back-to-back conversion system provides high reliability, fault tolerance, reduced dc-link capacitance, and hot-swap features. Furthermore, the proposed approach can be installed in existing grids feed by DGs from third parties, and does not require the change of commercial DGs to customized ones.

Appendix A

The calculation methods of all the terms in (3) are given as follows:

$$u_i = \begin{bmatrix} u_1 \\ u_2 \\ u_3 \end{bmatrix} = \begin{bmatrix} v_{Ad} - v_{\mathrm{DC}} m_{Ad} \\ v_{Aq} - v_{\mathrm{DC}} m_{Aq} \\ 0 \end{bmatrix}, \quad g_1(x) = \begin{bmatrix} \frac{1}{L_A} & 0 & 0 \end{bmatrix}$$

$$g_2(x) = \begin{bmatrix} 0 & \frac{1}{L_A} & 0 \end{bmatrix}, \quad g_3(x) = \begin{bmatrix} 0 & 0 & 0 \end{bmatrix}$$

$$\beta = \frac{1}{R_p} = \beta_n + \Delta\beta, \quad \Delta f(x) = \begin{bmatrix} 0 & 0 & -\frac{2\Delta\beta v_{\mathrm{DC}}^2}{C} \end{bmatrix}^T$$

$$\Delta f(x) = \begin{bmatrix} -\frac{R_A}{L_A} i_{Ad} + \omega_A i_{Aq} \\ -\frac{R_A}{L_A} i_{Aq} - \omega_A i_{Ad} \\ \frac{3}{C}\left(v_{Ad} i_{Ad} + v_{Aq} i_{Aq}\right) - \frac{2\beta_n v_{\mathrm{DC}}^2}{C} - \frac{2P_{\mathrm{load}}}{C} \end{bmatrix}$$

where L_A is the inductance, $\Delta\beta$ is the uncertainty, $g_1(x)$, $g_2(x)$, $g_3(x)$, $\bar{f}(x)$ and $\Delta f(x)$ are continuously differentiable functions.

Appendix B

The calculation methods of all the terms in (4) to (8) are given as follows, and the symbol "L" represents the Lee derivative

$$L_{\bar{f}} h_1(x) = \frac{3}{C}\left(v_{Ad} i_{Ad} + v_{Aq} i_{Aq}\right) - \frac{2\beta_n v_{DC}^2}{C^2} - \frac{2P_{\mathrm{load}}}{C},$$

$$L_{g_2} h_2(x) = 0, \quad G_3 = 1$$

$$L_{\Delta f} h_1(x) = -\frac{2\Delta\beta v_{\mathrm{DC}}^2}{C^2}, \quad L_{g_1} h_1(x) = L_{g_2} h_1(x) = 0,$$

$$L_{\Delta f} L_{\bar{f}} h_1(x) = \frac{4\beta_n v_{\mathrm{DC}}^2}{C^2}\Delta\beta$$

$$L_{g_1} L_{\bar{f}} h_1(x) = \frac{3 v_{Ad}}{L_A C}, \quad L_{g_2} L_{\bar{f}} h_1(x) = \frac{3 v_{Aq}}{L_A C},$$

$$L_{g_1} h_2(x) = \frac{1}{L_A}, \quad L_{\Delta f} h_2(x) = 0$$

$$L_{\bar{f}}^2 h_1(x) = \frac{3\left(v_{Ad} f_1(x) + v_{Aq} f_2(x)\right)}{C} - \frac{2\beta_n}{C}\bar{f}_3(x),$$

$$f_1(y_1) = 0, \quad G_1 = 1$$

$$L_{\bar{f}} h_2(x) = -\frac{R_A}{L_A} i_{Ad} + \omega_A i_{Aq}, \quad \phi_1^T(y_1) = -\frac{2v_{\mathrm{DC}}^2}{C},$$

$$f_2(y_1, y_2) = L_{\bar{f}}^2 h_1(x)$$

$$G_2 = 1, \quad \phi_2^T(y_1, y_2) = \frac{4\beta_n v_{\mathrm{DC}}^2}{C}, \quad f_3(y_3) = L_{\bar{f}} h_2(x),$$

$$\phi_3^T(y_3) = 0$$

$$L_f h_4(x) = -\frac{R_B^2}{L_B} i_{Bd} + R_B \omega_B i_{Bq},$$

$$L_f h_5(x) = -\frac{R_B^2}{L_B} i_{Bq} - R_B \omega_B i_{Bd}$$

$$L_{g4}h_4(x) = L_{g5}h_5(x) = \frac{R_B}{L_B}.$$

APPENDIX C

TABLE II
EXPERIMENTAL TEST SYSTEM PARAMETERS

System Quantities			Values
DGs			
DC voltage			$V_{dc}1 = V_{\mathrm{dc}2} = V_{\mathrm{dc}3} = 400$ V
Rated power (DGa1-small WTG)			$P_{DGa1-rated} = 5kW$
Rated power (DGa2-Battery bank)			$P_{DGa2-rated} = 3$ kW
Rated power (DGa1-PV array)			$P_{DGc1-rated} = 2$ kW
Loads	Load1	Rated voltage	220 V rms (L-N)
		Rated frequency	50 Hz
		Load power	2–3 kW, 1–2 kVar
	Load2	Rated voltage	220 Vrms (L-N)
		Rated frequency	50 Hz
		Load power	2.5–5 kW, 1–2 kVar
	Load3	Rated voltage rated frequency load power	220 V rms (L-N) 50 Hz 1 kW, 1 kVar
PSU system Droop controllers			$m_1 = 6 \times 10^{-5}, n_1 = 1 \times 10^{-3},$
			$m_2 = 9 \times 10^{-5}, n_2 = 1.5 \times 10^{-3},$ $m_3 = 6 \times 10^{-5}, n_3 = 1 \times 10^{-3}$
Rated power			4 kVA
DC-link voltage			$V_{dc} = 400$ V
Interlinked inductance			$L_A, L_B = 4$ mH,
			$R_A, R_B = 330$ mΩ

REFERENCES

[1] G. Pepermans, J. Driesen, D. haeseldonckx, R. Belmans, and W. D'haeseleer, "Distributed generation: Definition, benefits and issues," *Energy Policy*, vol. 33, no. 6, pp. 787–798, Apr. 2005.

[2] M. Hua, H. Hu, Y. Xing, and J. M. Guerrero, "Multilayer control for inverters in parallel operation without intercommunications," *IEEE Trans. Power Electron.*, vol. 27, no. 8, pp. 3651–3663, Aug. 2012.

[3] C. A. Platero, C. Nicolet, J. A. Sanchez, and B. Kawkabani, "Increasing wind power penetration in autonomous power systems through no-flow operation of Pelton turbines," *Renew. Energy*, vol. 68, pp. 515–523, Aug. 2014.

[4] X. Guan, Z. Xu, and Q. S. Jia, "Energy-efficient buildings facilitated by microgrid," *IEEE Trans. Smart Grid.*, vol. 1, no. 3, pp. 243–252, Dec. 2010.

[5] C. Chen, S. Duan, T. Cai, B. Liu, and G. Hu, "Smart energy management system for optimal microgrid economic operation," *IET Renew. Power Gen.*, vol. 5, no. 3, pp. 258–267, May 2011.

[6] S. Anand, B. G. Fernandes, and J. M. Guerrero, "Distributed control to ensure proportional load sharing and improve voltage regulation in low-voltage dc microgrids," *IEEE Trans. Power Electron.*, vol. 28, no. 4, pp. 1900–1913, Apr. 2013.

[7] D. Ahmadi and J. Wang, "Online selective harmonic compensation and power generation with distributed energy resources," *IEEE Trans. Power Electron.*, vol. 29, no. 7, pp. 3738–3747, Jul. 2014.

[8] J. M. Guerrero, P. C. Loh, T. Lee, and M. Chandorkar, "Advance control architectures for intelligent microgrids—Part II: Power quality, energy storage, and AC/DC microgrids," *IEEE Trans. Ind. Electron.*, vol. 60, no. 4, pp. 1263–1270, Apr. 2013.

[9] F. Shahnia, R. Majumder, A. Ghosh, G. Ledwic, and F. Zare, "Load sharing and power quality enhanced operation of a distributed microgrid," *IET Renew. Power Gen.*, vol. 3, no. 2, pp. 109–119, Jun. 2009.

[10] I. Y. Chung, W. Liu, D. A. Cartes, E. G. Collins, and S. I. Moon, "Control methods of inverter-interfaced distributed generators in a microgrid system," *IEEE Trans. Ind. Appl.*, vol. 46, no. 3, pp. 1078–1088, May/Jun. 2010.

[11] A. T. Gullberg, D. Ohlhorst, and M. Schreurs, "Towards a low carbon energy future-renewable energy cooperation between Germany and Norway," *Renew. Energy*, vol. 68, pp. 216–222, Aug. 2014.

[12] C. N. Rowe, T. J. Summers, R. E. Betz, D. J. Cornforth, and T. G. Moore, "Arctan power-frequency droop for improved microgrid stabillity," *IEEE Trans. Power Electron.*, vol. 28, no. 8, pp. 3747–3759, Aug. 2013.

[13] J. C. Vasquez, J. M. Guerrero, A. Luna, P. Rodríguez, and R. Teodorescu, "Adaptive droop control applied to voltage-source inverters operating in grid-connected and islanded modes," *IEEE Trans. Ind. Electron.*, vol. 56, no. 10, pp. 4088–4096, Oct. 2009.

[14] N. Pogaku, M. Prodanovic, and T. C. Green, "Modeling, analysis and testing of autonomous operation of an inverter-based microgrid," *IEEE Trans. Power Electron.*, vol. 22, no. 2, pp. 613–625, Mar. 2007.

[15] Q.-C. Zhong, "Robust droop controller for accurate proportional load sharing among inverters operated in parallel," *IEEE Trans. Ind. Electron.*, vol. 60, no. 4, pp. 1281–1290, Apr. 2013.

[16] S. Zhang, S. Jiang, X. Lu, B. Ge, and F. Z. Peng, "Resonance issues and damping techniques for grid-connected inverters with long transmission cable," *IEEE Trans. Power Electron.*, vol. 29, no. 1, pp. 110–120, Jan. 2014.

[17] E. Barklund, N. Pogaku, M. Prodanovic, C. Hernandez-Aramburo, and T. C. Green, "Energy management in autonomous microgrid using stability-constrained droop control of inverters," *IEEE Trans. Power Electron.*, vol. 23, no. 5, pp. 2346–2352, Sep. 2008.

[18] Y. A.-R. I. Mohamed and E. F. El-Saadany, "Adaptive decentralized droop controller to preserve power sharing stability of paralleled inverters in distributed generation microgrids," *IEEE Trans. Power Electron.*, vol. 23, no. 6, pp. 2806–2816, Nov. 2008.

[19] C. Bao, X. Ruan, X. Wang, W. Li, D. Pan, and K. Weng, "Step-by-step controller design for LCL-type grid-connected inverter with capacitor-current-feedback active-damping," *IEEE Trans. Power Electron.*, vol. 29, no. 3, pp. 1239–1253, Mar. 2014.

[20] Y. W. Li and C. N. Kao, "An accurate power control strategy for power-electronics-interfaced distributed generation units operating in a low-voltage multibus microgrid," *IEEE Trans. Power Electron.*, vol. 24, no. 12, pp. 2977–2988, Dec. 2009.

[21] W. Yao, M. Chen, J. Matas, J. M. Guerrero, and Z.-M. Qian, "Design and analysis of the droop control method for parallel inverters considering the impact of the complex impedance on the power sharing," *IEEE Trans. Ind. Electron.*, vol. 58, no. 2, pp. 576–588, Feb. 2011.

[22] J. He and Y. W. Li, "An enhanced microgrid load demand sharing strategy," *IEEE Trans. Power Electron.*, vol. 27, no. 9, pp. 3984–3995, Sep. 2012.

[23] K. S. Parlak, M. Ozdemir, and M. Timur Aydemir, "Active and reactive power sharing and frequency restoration in a distributed power system consisting of two UPS units," *Elect. Power Energy Syst.*, vol. 31, no. 5, pp. 220–226, Jun. 2009.

[24] J. M. Guerrero, M. Chandorkar, T. Lee, and P. C. Loh, "Advance control architectures for intelligent microgrids—Part I: Decentralized and hierarchical control," *IEEE Trans. Ind. Electron.*, vol. 60, no. 4, pp. 1254–1262, Apr. 2013.

[25] J. Vasquez, J. M. Guerrero, M. Savaghebi, J. Eloy-Garcia, and R. Teodorescu, "Modeling, analysis, and design of stationary reference frame droop controlled parallel three-phase voltage source inverters," *IEEE Trans. Ind. Electron.*, vol. 60, no. 4, pp. 1271–1280, Apr. 2013.

[26] Q. Shafiee, J. Guerrero, and J. C. Vasquez, "Distributed secondary control for islanded microgrids—A novel approach," *IEEE Trans. Power Electron.*, vol. 29, no. 2, pp. 1018–1031, Feb. 2014.

[27] R. Majumder, A. Ghosh, G. Ledwich, and F. Zare, "Power management and power flow control with back-to-back converters in a utility connected microgrid," *IEEE Trans. Power Syst.*, vol. 25, no. 2, pp. 821–834, May. 2010.

[28] H. Akagi and R. Kitada, "Control and design of a modular multilevel cascade BTB system using bidirectional isolated DC/DC converters," *IEEE Trans. Power Electron.*, vol. 26, no. 9, pp. 2457–2464, Sep. 2011.

[29] X. Lu, J. M. Guerrero, K. Sun, J. C. Vasquez, R. Teodorescu, and L. Huang, "Hierarchical control of parallel AC-DC converter interfaces for hybrid microgrids," *IEEE Trans. Smart Grid.*, vol. 5, no. 2, pp. 683–692, Mar. 2014.

[30] R. Majumder, A. Ghosh, G. Ledwich, and F. Zare, "Operation and control of single phase micro-sources in a utility connected grid," in *Proc. IEEE Power Energy Soc. Gen. Meeting*, 2009, pp. 1–7.
[31] R. Majumder, "Reactive power compensation in single phase operation of microgrid," *IEEE Trans. Ind. Electron.*, vol. 60, no. 4, pp. 1403–1416, Apr. 2013.
[32] Z. Shu, S. Xie, and Q. Li, "Single-phase back-to-back converter for active power balancing, reactive power compensation, and harmonic filtering in traction power system," *IEEE Trans. Power Electron.*, vol. 26, no. 2, pp. 334–343, Feb. 2011.
[33] S. Chakraborty and M. G. Simoes, "Experimental evaluation of active filtering in a single-phase high-frequency AC microgrid," *IEEE Trans. Energy Convers.*, vol. 24, no. 3, pp. 673–682, Sep. 2009.
[34] J. He, Y. W. Li, J. M. Guerrero, F. Blaabjerg, and J. C. Vasquez, "An islanding microgrid power sharing approach using enhanced virtual impedance control scheme," *IEEE Trans. Power Electron.*, vol. 28, no. 11, pp. 5272–5282, Nov. 2013.
[35] B. B. Johnson, S. V. Dhople, A. O. Hamadeh, and P. T. Krein, "Synchronization of parallel single-phase inverters with virtual oscillator control," *IEEE Trans. Power Electron.*, vol. 29, no. 11, pp. 6124–6138, Nov. 2014.
[36] P. Rodriguez, A. Luna, I. Candela, R. Mujal, R. Teodorescu, and F. Blaabjerg, "Multiresonant frequency-locked loop for grid synchronization of power converters under distorted grid conditions," *IEEE Trans. Ind. Electron.*, vol. 58, no. 1, pp. 127–138, Jan. 2011.
[37] H. Zhang, D. Liu, Y. Luo, and D. Wang, *Adaptive Dynamic Programming for Control-Algorithms and Stability*. London, U.K.: Springer-Verlag, 2013.
[38] B. Parkhideh and S. Bhattacharya, "Vector-controlled voltage-source-converter-based transmission under grid disturbances," *IEEE Trans. Power Electron.*, vol. 28, no. 2, pp. 661–672, Feb. 2013.
[39] A. Allag, M. Y. Hammoudi, S. M. Mimoune, M. Y. Ayad, M. Becherif, and A. Miraoui, "Tracking control via adaptive backstepping approach for a three phase PWM AC-DC converter," in *Proc. IEEE Int. Symp. Ind. Electron.*, 2007, pp. 371–376.
[40] H. Zhang, L. Cai, and Z. Bien, "A fuzzy basis function vector-based multivariable adaptive controller for nonlinear systems," *IEEE Trans. Syst. Man, Cybern. B, Cybern.*, vol. 30, no. 1, pp. 210–217, Feb. 2000.
[41] J. Niiranen, R. Komsi, M. Routimo, T. Lähdeaho, and S. Antila, "Experiences from a back-to-back converter fed village microgrid," in *Proc. Innovative Smart Grid Technol. Conf. Eur.*, vol. 1, no. 5, pp. 11–13, Oct. 2010.
[42] H. Zhang, C. Qing, and Y. Luo, "Neural-network-based constrained optimal control scheme for discrete-time switched nonlinear system using dual heuristic programming," *IEEE Trans. Autom. Sci. Eng.*, vol. 11, no. 3, pp. 839–849, Jul. 2014.

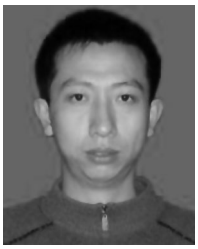

Qiuye Sun (M'12) received the B.S. degree in power system and its automation from the Northeast Dianli University of China, Jilin City, China, in 2000, the M.S. degree in power electronics and power drives, and the Ph.D. degree in control theory and control engineering from the Northeastern University, Shenyang, China, in 2004 and 2007, respectively.

He joined the School of Information Science and Engineering, Northeastern University, Shenyang, China, in 2007. Since 2014, he has been a Full Professor with the Institute of Electric of Automation, School of Information Science and Engineering, Northeastern University, China. His main research interests include optimization and control of smart grid, and network control of distributed generation system, microgrids, and Energy Internet. He has authored and coauthored more than 60 journal and conference papers, 8 monographs, and coinvented 65 patents.

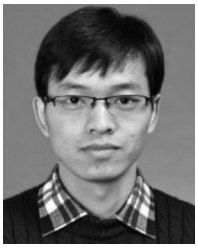

Jianguo Zhou was born in Yunnan, China, in 1987. He received the B.S. degree in automation, and the M.S. degree in control theory and control engineering from the Northeastern University, Shenyang, China, in 2011 and 2013, respectively, where he is currently working toward the Ph.D. degree in control theory and control engineering.

His current research interests include power electronics, hierarchical and distributed cooperative control, and power quality improvement of microgrids, and synchronization of complex/multiagent networks and their applications in microgrids and Energy Internet.

Josep M. Guerrero (S'01–M'04–SM'08–F'14) received the B.S. degree in telecommunications engineering, the M.S. degree in electronics engineering, and the Ph.D. degree in power electronics from the Technical University of Catalonia, Barcelona, in 1997, 2000, and 2003, respectively.

Since 2011, he has been a Full Professor with the Department of Energy Technology, Aalborg University, Denmark, where he is responsible for the Microgrid Research Program. Since 2012, he has been a Guest Professor at the Chinese Academy of Science and the Nanjing University of Aeronautics and Astronautics; and since 2014, he has been the Chair Professor in Shandong University. His research interests include different microgrid aspects, including power electronics, distributed energy-storage systems, hierarchical and cooperative control, energy management systems, and optimization of microgrids and islanded minigrids.

Prof. Guerrero is an Associate Editor for the IEEE TRANSACTIONS ON POWER ELECTRONICS, the IEEE TRANSACTIONS ON INDUSTRIAL ELECTRONICS, and the IEEE INDUSTRIAL ELECTRONICS MAGAZINE, and an Editor for the IEEE TRANSACTIONS ON SMART GRID. He has been Guest Editor of the IEEE TRANSACTIONS ON POWER ELECTRONICS Special Issues: Power Electronics for Wind Energy Conversion and Power Electronics for Microgrids; the IEEE TRANSACTIONS ON INDUSTRIAL ELECTRONICS Special Sections: Uninterruptible Power Supplies systems, Renewable Energy Systems, Distributed Generation and Microgrids, and Industrial Applications and Implementation Issues of the Kalman Filter; and the IEEE TRANSACTIONS ON SMART GRID Special Issue on Smart DC Distribution Systems. He was the Chair of the Renewable Energy Systems Technical Committee of the IEEE Industrial Electronics Society. In 2014, he received Thomson Reuters as ISI Highly Cited Researcher, and in 2015 he was elevated as IEEE Fellow for contributions to "distributed power systems and microgrids."

Huaguang Zhang (M'03–SM'04–F'14) received the B.S. and M.S. degrees in control engineering from Northeast Dianli University of China, Jilin City, China, in 1982 and 1985, respectively. He received the Ph.D. degree in thermal power engineering and automation from Southeast University, Nanjing, China, in 1991.

He joined the Department of Automatic Control, Northeastern University, Shenyang, China, in 1992, as a Postdoctoral Fellow for 2 years. Since 1994, he has been a Professor and the Head of the Institute of Electric Automation, School of Information Science and Engineering, Northeastern University, Shenyang, China. His main research interests include fuzzy control, stochastic system control, neural networks-based control, nonlinear control, and their applications. He has authored and coauthored more than 280 journal and conference papers, six monographs, and coinvented 90 patents.

Dr. Zhang is the Chair of the Adaptive Dynamic Programming and Reinforcement Learning Technical Committee on the IEEE COMPUTATIONAL INTELLIGENCE SOCIETY. He is an Associate Editor of *Automatica*, the IEEE TRANSACTIONS ON NEURAL NETWORKS, the IEEE TRANSACTIONS ON CYBERNETICS, and NEUROCOMPUTING, respectively. He was an Associate Editor of the IEEE TRANSACTIONS ON FUZZY SYSTEMS (2008–2013). He received the Outstanding Youth Science Foundation Award from the National Natural Science Foundation Committee of China in 2003. He was named the Cheung Kong Scholar by the Education Ministry of China in 2005. He received the IEEE TRANSACTIONS ON NEURAL NETWORKS 2012 Outstanding Paper Award.